Rapid Communications

Magnon scattering in the transport coefficients of CoFe thin films

S. Srichandan,[1] S. Wimmer,[2] S. Pöllath,[1] M. Kronseder,[1] H. Ebert,[2] C. H. Back,[1] and C. Strunk[1]
[1]*Institute of Experimental and Applied Physics, University of Regensburg, D-93040 Regensburg, Germany*
[2]*Department of Chemistry, Physical Chemistry, Ludwig-Maximilians-Universität, D-81377 Munich, Germany*

(Received 5 January 2018; published 13 July 2018)

Resistivity ρ, thermopower $\mathcal{S}$, and thermal conductivity κ were measured simultaneously on a set of CoFe alloy films. Variation of the Co content x_{Co} allows for a systematic tuning of the Fermi level through the band structure, and the study of the interplay between electronic and magnetic contributions to the transport coefficients. While band-structure and magnon effects in ρ and κ are rather weak, they turn out to be very significant in $\mathcal{S}$. A decomposition of $\mathcal{S}$ into Mott and magnon drag contributions results in a systematic evolution between the two limiting cases of pure Fe and pure Co. At low temperatures, we find an interesting sign change of the curvature of $\mathcal{S}(T)$ that indicates a corresponding sign change of the magnon drag.

DOI: 10.1103/PhysRevB.98.020406

Spintronics [1,2] and more recently spin caloritronics [3,4] have sparked interest in the fundamental transport properties of ferromagnetic thin films since devices engineered from ultrathin ferromagnetic layer stacks have a potential for technological applications. While the measurement and interpretation of electrical transport parameters is rather straightforward, even for thin ferromagnetic films [5], the measurements and interpretation of their thermal, thermoelectric, and magnetothermoelectric counterparts is much more difficult. However, the optimization of spintronic and spin-caloritronic devices depends on the accurate knowledge of the various thermal transport parameters as well as the parameters governing the relaxation mechanisms for electrons, phonons, and magnons in thin-film ferromagnetic materials. Similarly, the exploitation of magnon transport in temperature gradients for the transmission and processing of information [6,7] depends on the understanding and quantitative knowledge of their thermoelectric and thermomagnetic properties.

So far only a few experiments have addressed the interplay of the magnetothermoelectric transport parameters using the modern toolbox of nanotechnology [8–15]; these were mainly focused on the prototypical ferromagnet permalloy while systematic investigations as a function of alloy composition are still lacking. On the theory side, significant progress has been made in the description of spin-dependent transport phenomena. The use of *ab initio* theory in combination with a realistic description of alloys [16–19] allows now for a fresh look at the transport properties of ferromagnetic alloys. Of particular interest is the prediction of Flebus *et al.* [20], who pointed out that besides the usual diffusion term in the thermoelectric power (TEP), two contributions compete in the *magnon drag*: one of hydrodynamic origin that drives majority carriers towards the cold side of the sample, and a second one in the opposite direction. The second contribution arises from the accumulation of spin Berry phase in a time-dependent magnetization texture [21], caused here by the thermally excited spin waves.

Experimental evidence for magnon drag effects in the TEP has been reported for elemental Fe [22] and Cr [23] bulk samples. Only very recently was the topic taken up again by Watzman *et al.* [24], who attributed an important contribution to the TEP and the Nernst coefficient of elemental Fe and Co to magnon scattering. Interestingly, the sign of the presumed magnon contribution to the TEP is opposite for both metals. Hence the natural questions arise, what is the reason for this sign change and what is the evolution of the TEP in CoFe alloys between the two elements. With varying composition, not only does the electron density, but also the phonon and magnon dispersion relations change. This affects all sources of scattering processes for the electrons and thus the temperature dependence of the transport coefficients. So far only the electric and spin transport in CoFe alloys were recently carefully studied, and the spin-wave damping parameters $\alpha(x_{\mathrm{Co}})$ measured [25,26].

Here, we investigate a series of CoFe alloy films on SiN_x-based suspended microcalorimeters. Simultaneous measurements of several transport coefficients, i.e., the resistivity $\rho(T)$, the TEP $\mathcal{S}(T)$, and the thermal conductivity $\kappa(T)$, are performed in a wide temperature range of 25–300 K on the very same films. In this way, we directly probe the variation of the spin-polarized band structure and the relevant scattering mechanisms with the Co content, and the evolution of magnon scattering in different observables. We find evidence for magnon scattering effects most clearly in the TEP. The magnon drag contribution $\mathcal{S}_{\mathrm{mag}}(T,x_{\mathrm{Co}}) \propto T^{3/2}$ systematically decreases with x_{Co}, and changes sign near $x_{\mathrm{Co}} \simeq 0.6$.

To fabricate the samples, (60–80)-nm-thick CoFe films are deposited as rectangles (116 μm × 60 μm) by molecular beam epitaxy in an ultrahigh vacuum chamber on 500-nm-thick SiN_x membranes [light blue in Fig. 1(b)] with an area of 500 μm × 500 μm. The film is examined using atomic force microscopy (AFM) for the determination of the surface roughness, by x-ray photoelectron spectroscopy for stoichiometry determination, and by electron diffraction for structural analysis. The crystal structure for $x_{\mathrm{Co}} = 0.3$ turns out to be bcc while for $x_{\mathrm{Co}} = 0.8$ we find a clear admixture of fcc precipitations, similar to the findings in Ref. [25].

Next, the contact leads and thermometers are patterned using *e*-beam lithography (EBL) and a deposition of 50 nm

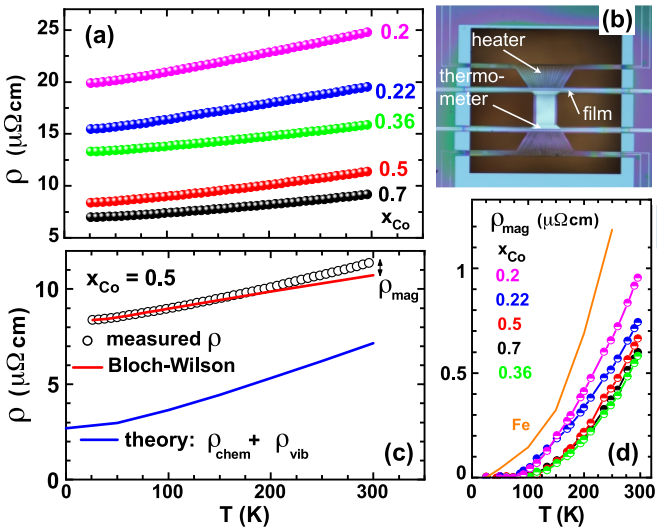

FIG. 1. (a) Resistivity $\rho(T)$ for several values of Co content x_{Co}. (b) Optical image of a typical device. (c) The phonon contribution to the resistivity for $x_{\mathrm{Co}} = 0.5$ (open circles) fitted to a Bloch-Wilson function for $T \leqslant 100$ K (red line). Double-headed arrow: Estimated magnon contribution to $\rho(T)$. Blue line: Calculated resistivity taking into account chemical disorder and lattice vibrations for $x_{\mathrm{Co}} = 0.5$ (see text). (d) Estimated ρ_{mag} for all samples (dots) vs temperature with ρ_{mag} for bulk Fe from Ref. [29] (orange line).

of Al. The thermometers are 100-μm-long and 1.5-μm-wide wires. The contact leads are also 1.5 μm wide. In a second EBL step, two symmetrically placed meander heater structures are patterned in a 40-nm-thick $Au_{60}Pd_{40}$ film. Finally, the parts of the membranes that do not support the metal structures [black area in Fig. 1(b)] are reactively etched using a CHF_3/O_2 plasma for 10 min, leaving a freely suspended SiN_x bridge. (More details on the film characterization and sample layout are given in the Supplemental Material [27].)

The measurements were performed in a helium flow cryostat in vacuum. Radiation losses are minimized by virtue of a radiation shield at the sample temperature. All resistances were measured in a four-terminal configuration. The TEP $\mathcal{S}(T)$ and the thermal conductance $K(T)$ were determined simultaneously by measuring the temperature difference ΔT between the ends of the bridge versus heater current such that $\Delta T/T < 0.01$. The corresponding thermovoltage V_{th} is measured using a nanovoltmeter and the TEP is extracted from the slope of $V_{\mathrm{th}}(\Delta T)$. The total thermal conductance $K = P_{\mathrm{H}}/\Delta T$ includes the thermal conductances K_{B} and K_{L} of the bridge and the lead sections, respectively. P_{H} is the heater power. In the absence of radiation or convection losses, the one-dimensional (1D) heat diffusion equation can be solved to find K_{B} and K_{L} independently [15,28]. K_{B} contains both K_{CoFe} and K_{SiN_x}. To determine K_{SiN}, we have prepared four devices with bare SiN_x. From the thermal conductance $K_{\mathrm{CoFe}} = K_{\mathrm{B}} - K_{\mathrm{SiN}_x}$ we calculate the thermal conductivity $\kappa_{\mathrm{CoFe}} = \kappa$ using the known dimensions of the film for all the samples with different compositions. The maximal uncertainty of κ resulting from the variance of K_{SiN} between the different SiN_x membranes is $\simeq$7.5 W/(K m).

In Fig. 1(a) the resistivity $\rho(T)$ of all five samples is plotted as a function of temperature. The resistivity is highest for $x_{\mathrm{Co}} = 0.20$ and decreases monotonically with the addition of Co. This decrease is mainly a consequence of the increase in electron number. In addition, at $x_{\mathrm{Co}} \simeq 0.2$, a d-like band crosses the Fermi surface, resulting in a maximal $\rho(x_{\mathrm{Co}})$ (for more details and a comparison with earlier experiments, see the Supplemental Material [27]).

Next, we evaluate the magnon contribution ρ_{mag} to $\Delta\rho(T)$. According to the analysis of Refs. [29,30], ρ_{mag} becomes sizable only above $T \simeq 100$ K. Hence, we first determine the phonon contribution by fitting the measured $\rho(T)$ to a Bloch-Wilson (BW) function [27] from 26 up to 100 K. An example is shown in Fig. 1(c) for $x_{\mathrm{Co}} = 0.5$. Extrapolating to 300 K, we can evaluate the magnon contribution $\rho_{\mathrm{mag}}(T)$ by subtracting the BW fit from the measured $\rho(T)$. The results are plotted in Fig. 1(d): $\rho_{\mathrm{mag}}(T)$ gradually decreases with increasing x_{Co} (with $x_{\mathrm{Co}} = 0.36$ being an outlier). The magnon contribution is at most 6.5% of ρ at room temperature for $x_{\mathrm{Co}} = 0.20$, corresponding to about 1/5 of the phonon contribution. The magnitude and temperature dependence of $\rho_{\mathrm{mag}}(T)$ are quite comparable to that of elemental Fe [29] [orange line in Fig. 1(d)]. The blue line in Fig. 1(c) shows a first-principles calculation of $\rho(T)$ for $x_{\mathrm{Co}} = 0.5$ within the Kubo formalism accounting for chemical disorder via the coherent-potential approximation (CPA) alloy theory and for thermal lattice vibrations via the alloy analogy model [16]. The calculation underestimates the absolute values and overestimates the slope of $\rho(T)$ both by a factor of $\simeq$2 as it does not include the considerable structural disorder.

Next, we present the results for the thermopower in Fig. 2(a), which constitutes our main result. At high temperatures, $\mathcal{S}(T)$ is negative and varies roughly linearly with temperature. Note that the approximately linear parts at $T > 100$ K do not extrapolate to $\mathcal{S} = 0$ at $T = 0$, as opposed to the expectation from the Mott law. At low temperatures $\mathcal{S}(T)$ is not linear. This implies that $\mathcal{S}(T)$ cannot be described by a Mott-like dependence alone, but additional nonlinear contributions have to be present. Moreover, the curvature clearly changes sign: It is positive for lower Co content, i.e., $x_{\mathrm{Co}} = 0.2$ and 0.22, but negative for $x_{\mathrm{Co}} = 0.7$ and 0.5. At the lowest temperatures, $\mathcal{S}(T, x_{\mathrm{Co}} = 0.7)$ becomes slightly positive.

By fitting the high-temperature part of $\mathcal{S}(T)$ to a Mott-like term linear in T, and a second term proportional to $T^{3/2}$, we can decompose the TEP according to

$$\mathcal{S}(T) = \mathcal{S}'_{\mathrm{Mott}} T + \mathcal{S}'_{\mathrm{mag}} T^{3/2} + \mathcal{S}_{\mathrm{res}}(T). \qquad (1)$$

The coefficients $\mathcal{S}'_{\mathrm{Mott}}(x_{\mathrm{Co}})$ and $\mathcal{S}'_{\mathrm{mag}}(x_{\mathrm{Co}})$ describe the dependencies of the Mott-like part $\mathcal{S}_{\mathrm{Mott}}(T)$ and magnon drag contribution $\mathcal{S}_{\mathrm{mag}}(T)$ on x_{Co}. We have verified that these coefficients are robust against a change of the fit interval within 100–300 K. Below 100 K a much smaller residual contribution $\mathcal{S}_{\mathrm{res}}(T) \lesssim 1$ μV/K remains (see Supplemental Material [27]).

Figure 2(b) shows the Mott-like contribution that is proportional to T. The absolute values $|\mathcal{S}_{\mathrm{Mott}}(T)|$ decrease with increasing Co content, i.e., with increasing electron density, which is consistent with the corresponding trend seen in $\rho(T)$. The values of $\mathcal{S}'_{\mathrm{Mott}}$ contain a small contribution $\mathcal{S}'_{\mathrm{Mott,Al}} = 3.7$ nV/K^2 from the diffusion thermopower of the Al leads [31].

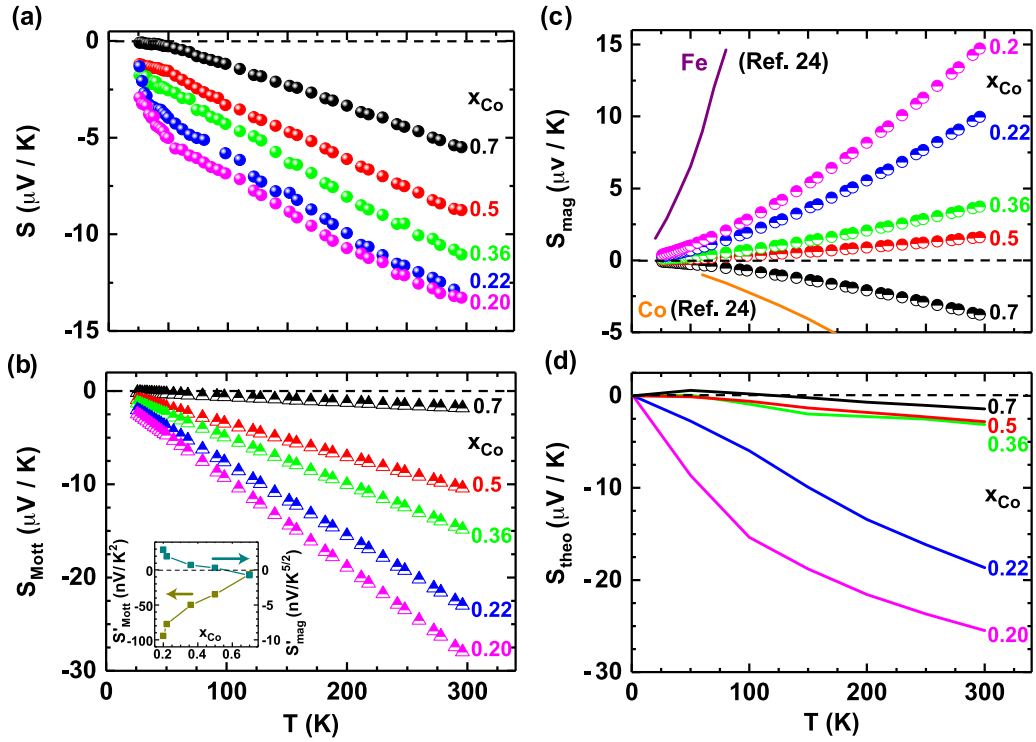

FIG. 2. (a) Measured thermopower vs temperature for all Co_xFe_{1-x} samples from 26 to 296 K, labeled on the right by at. % Co. (b) Mott-like contribution $\mathcal{S}_{\rm Mott}(T)$ (half-solid triangles) as a function of temperature. Inset: $\mathcal{S}_{\rm Mott}$ and $\mathcal{S}_{\rm mag}$ vs at. % Co at 296 K. (c) Magnon drag $\mathcal{S}_{\rm mag}(T) \propto T^{3/2}$ contribution (half-solid circles); literature values for bulk Co and Fe [24] are shown as lines. (d) Calculated thermopower taking into account chemical and vibrational disorder.

On the other hand, we find a substantial nonlinear contribution $\mathcal{S}_{\rm mag}(T)$ that increases proportionally to the magnon number and is as large as 13.5 μV/K at 296 K for the film with $x_{\rm Co} = 0.2$ [Fig. 2(c)]. The sign of the coefficient $\mathcal{S}'_{\rm mag}$ is positive for $x_{\rm Co} \lesssim 0.5$ and negative for $x_{\rm Co} = 0.7$ (inset). This is reflected in the sign change of $\mathcal{S}_{\rm mag}(T)$ from positive for the Fe-rich to negative for the Co-rich alloys, which agrees with $\mathcal{S}_{\rm mag}$ for the case of elemental Fe and Co [24] at these temperatures. The inset in Fig. 2(b) shows the evolution of the coefficients $\mathcal{S}'_{\rm Mott}$ and $\mathcal{S}'_{\rm mag}$ with $x_{\rm Co}$.

In ferromagnets, the magnon drag contribution to the TEP has a $T^{3/2}$ dependence at low T, provided that $T > \Delta_{\rm mag}/k_{\rm B}$ ($\Delta_{\rm mag}$ being the gap in the magnon dispersion relation), which reflects the variation of magnon density and specific heat with T. The magnon drag peak normally occurs at a temperature roughly one fifth to one half of the Curie temperature $T_{\rm C}$ of the material [22]. Due to the high $T_{\rm C}$ of the studied CoFe alloys the maximal magnon drag for our films is expected above the temperature range investigated here. The magnon damping in CoFe alloys is comparable to or even lower than those of the pure elements [26]. Hence, alloying does not lead to a substantial shortening of the magnon lifetime, and magnon drag can survive in the presence of disorder, in contrast to phonon drag [24].

The TEP can also be obtained from first-principles calculations [27]. The results are shown in Fig. 2(d). For the highest and lowest Co concentration the calculation can reproduce the size and systematics of the experimental data, but for intermediate concentrations it significantly underestimates both the measured TEP in Fig. 2(a) and the linear contribution to the TEP in Fig. 2(b). In this theory the curvature arises from the rapid variation of the energy-dependent conductivity when the d bands touch the Fermi energy around $x_{\rm Co} \simeq 0.2$ (see Supplemental Material for details [27]). At high temperatures, this requires one to go beyond the term linear in T in the Sommerfeld expansion. Taking into account also spin disorder further reduces $\mathcal{S}_{\rm theo}$. Given the significant curvature of the measured thermopower below 100 K, our experimental results cannot be explained by the diffusion contribution alone.

The computed suppression of $\mathcal{S}_{\rm theo}(x_{\rm Co} \lesssim 0.5)$ can, in part, be reverted by the presence of fcc precipitations with intrinsically larger absolute values of $\mathcal{S}_{\rm theo}$ and an opposite curvature [27,32]. The relevance of such precipitations is also corroborated by the behavior of the thermal conductivity (see below).

Most interesting is the sign change observed for $\mathcal{S}_{\rm mag}$ when $x_{\rm Co}$ is tuned from the Fe- to the Co-rich side. As already mentioned, recent theoretical work has calculated the spin-motive forces in presence of a magnetization texture [20]: (i) a Berry-phase contribution that drives the majority spins towards the hot end and is controlled by the adiabatic damping parameter β, and (ii) a hydrodynamic contribution that drives the majority spins towards the cold end and is controlled by the Gilbert damping α. A finite difference between majority- and minority-spin-motive force results in an electromotive force proportional to the magnon number (i.e., $\propto T^{3/2}$). The magnetic texture induced by a thermally excited magnon generates a magnon drag contribution to the TEP. The Gilbert damping $\alpha(x_{\rm Co})$ has been determined from ferromagnetic resonance experiments [26]. So far the analysis of our data using this strongly simplified model results in unphysically high values of

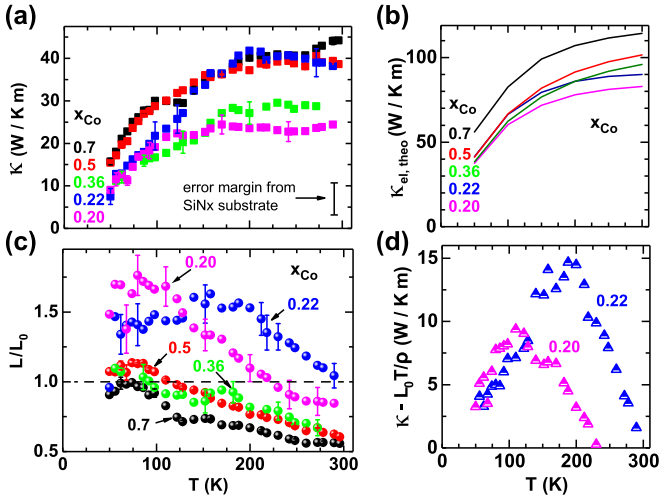

FIG. 3. (a) Measured thermal conductivity of the Co_xFe_{1-x} films. (b) Calculated electronic contribution to κ_{el} including elastic scattering on lattice vibrations. (c) Extracted Lorenz number L as a function of bath temperature. The horizontal line indicates the Sommerfeld value $L_0 = \pi^2/3 \cdot (k_B/e)^2$. (d) Positive deviations from the Wiedemann-Franz law using the measured resistivity of the films with low Co content.

β. On the other hand, the clear systematics that we observe calls for a more quantitative theoretical treatment of magnon drag.

Finally, we investigate the thermal conductivity κ in the films. As demonstrated in Fig. 3(a), $\kappa(T)$ increases with temperature and then saturates at high temperatures for all films. The individual curves are subjected to a $\pm 10\%$ random shift from the slightly varying background contribution of the different SiN_x membranes (see Supplemental Material [27]). The corresponding calculation of the electronic contribution $\kappa_{el}(T)$ including temperature-dependent vibrational disorder in Fig. 3(b) overall reproduces the systematics and the proportions for samples of different Co contents, with the exception that the monotonic increase of κ with x_{Co} observed in the calculated data is violated for $x_{Co} = 0.36$ at high T in our experiment. The absolute values of κ are overestimated by the very same factor of $\simeq 2$, by which the theory underestimates the electric resistivity in Fig. 1(c).

The Lorenz number $L(T) = \kappa(T)\rho(T)/T$ evaluated from the measured set of ρ and κ is shown in Fig. 3(c). We observe a significant violation of Wiedemann-Franz law (WFL, indicated by the horizontal line). Enhancement of L above L_0 is found for $x_{Co} = 0.22$, while L is smaller than L_0 for $x_{Co} = 0.7$ at all temperatures. For intermediate x_{Co}, $L > L_0$ at low T and vice versa at higher T. The positive deviation from WFL, i.e., $L > L_0$, is naturally explained by the contribution κ_{ph} from phonons to the thermal conductivity. In the investigated T regime the magnon contribution to κ is usually small compared to the phonon contribution [33]. Only in films without fcc precipitations ($x_{Co} = 0.2$ and 0.22) can one expect κ_{ph} to become significant, because such precipitations drastically shorten the phonon mean free path. Hence we estimate $\kappa_{ph} \simeq \kappa - TL_0/\rho$ [see Fig. 3(d); Supplemental Material [27]]; it shows clear maxima around 100 and 200 K, respectively, which resemble the well-known umklapp peak. They are shifted towards higher temperatures with respect to the phononic umklapp peak for pure Fe or Co.

The observed negative deviations from WFL can be explained by the gradual reduction of the phonon mean free path in films with $x_{Co} \gtrsim 0.36$. Besides suppressing κ_{ph}, the electronic contribution κ_{el} is known to be enhanced in the presence of inelastic ("vertical") scattering of electron with phonons [13,34], while these scattering events are not effective in the resistivity. In addition, it is known that $L < L_0$ for pure Co in this temperature range [35], and is thus in agreement with the behavior of $L(T)$ in Co-rich samples.

To summarize, simultaneous measurements of the electric, thermoelectric, and thermal transport coefficients performed on alloyed CoFe films have enabled us to understand the contribution from electrons, phonons, and magnons qualitatively and in part even quantitatively. In particular, the evolution of the thermopower indicates a possible interplay of diffusion and magnon drag contributions, the latter changing sign close to the center of the concentration range. A generalized Mott theory is also qualitatively consistent with the results. For the thermal conductivity a pronounced violation of the Wiedemann-Franz law is observed in structurally homogeneous samples with low Co content. A quantitative understanding of the observed systematic evolution of the thermoelectric power calls for a more elaborate theory.

The authors thank T. N. G. Meier for the XPS analysis, M. Zimmermann for AFM measurements, M. Vogel for COMSOL simulations, C. Sürgers for the x-ray characterization of the CoFe films, Y. Tserkovnyak and R. A. Duine for helpful comments on their theory, J. Zweck for support with the electron diffraction, and gratefully acknowledge financial support by the Deutsche Forschungsgemeinschaft (DFG) within the priority programme SpinCaT (SPP 1538) and the Bundesministerium für Bildung und Forschung (BMBF).

[1] I. Zutić, J. Fabian, and S. D. Sharma, Rev. Mod. Phys. **76**, 323 (2004).
[2] D. C. Ralph and M. D. Stiles, J. Magn. Magn. Mater. **320**, 1190 (2008).
[3] G. E. W. Bauer, A. H. MacDonald, and S. Maekawa, Solid State Commun. **150**, 459 (2010).
[4] S. R. Boona, R. C. Myers, and J. P. Heremans, Energy Environ. Sci. **7**, 885 (2014).
[5] *Spin Dependent Transport in Magnetic Nanostructures*, edited by S. Maekawa and T. Shinjo, Advances in Condensed Matter Science Vol. 3 (CRC Press, Boca Raton, FL, 2002).
[6] S. A. Nikitov *et al.*, Phys. Usp. **58**, 1002 (2015).
[7] L. J. Cornelisen, J. Liu, R. A. Duine, J. B. Youssef, and B. J. van Wees, Nat. Phys. **11**, 1022 (2015).
[8] D. W. Denlinger, E. N. Abarra, K. Allen, P. W. Rooney, M. T. Messer, S. K. Watson, and F. Hellman, Rev. Sci. Instrum. **65**, 946 (1994).
[9] A. Lopeandia, L. Cerdo, M. Clavaguera-Mora, L. R. Arana, K. Jensen, F. Munoz, and J. Rodriguez-Viejo, Rev. Sci. Instrum. **76**, 065104 (2005).
[10] M. N. Ou, T. J. Yang, S. R. Harutyunyan, Y. Y. Chen, C. D. Chen, and S. J. Lai, Appl. Phys. Lett. **92**, 063101 (2008).

[11] B. L. Zink, A. D. Avery, R. Sultan, D. Bassett, and M. R. Pufall, Solid State Commun. **150**, 514 (2010).

[12] D. W. Cooke, F. Hellman, J. R. Groves, B. M. Clemens, and S. Moyerman, Rev. Sci. Instrum. **82**, 023908 (2011).

[13] A. D. Avery, M. R. Pufall, and B. L. Zink, Phys. Rev. Lett. **109**, 196602 (2012).

[14] M. Schmid, S. Srichandan, D. Meier, T. Kuschel, J.-M. Schmalhorst, M. Vogel, G. Reiss, C. Strunk, and C. H. Back, Phys. Rev. Lett. **111**, 187201 (2013).

[15] R. Sultan, A. D. Avery, G. Stiehl, and B. L. Zink, J. Appl. Phys. **105**, 043501 (2009).

[16] H. Ebert, S. Mankovsky, K. Chadova, S. Polesya, J. Minár, and D. Ködderitzsch, Phys. Rev. B **91**, 165132 (2015).

[17] R. Kováčik, P. Mavropoulos, and S. Blügel, Phys. Rev. B **91**, 014421 (2015).

[18] M. Obstbaum, M. Decker, A. K. Greitner, M. Haertinger, T. N. G. Meier, M. Kronseder, K. Chadova, S. Wimmer, D. Ködderitzsch, H. Ebert, and C. H. Back, Phys. Rev. Lett. **117**, 167204 (2016).

[19] S. Meyer, Y.-T. Chen, S. Wimmer, M. Althammer, T. Wimmer, R. Schlitz, S. Geprägs, H. Huebl, D. Ködderitzsch, H. Ebert, G. E. W. Bauer, R. Gross, and S. T. B. Goennenwein, Nat. Mater. **16**, 977 (2017).

[20] B. Flebus, R. A. Duine, and Y. Tserkovnyak, Europhys. Lett. **115**, 57004 (2016).

[21] Y. Tserkovnyak and C. H. Wong, Phys. Rev. B **79**, 014402 (2009).

[22] F. J. Blatt, D. J. Flood, V. Rowe, P. A. Schroeder, and J. E. Cox, Phys. Rev. Lett. **18**, 395 (1967).

[23] A. L. Trego and A. R. Mackintosh, Phys. Rev. **166**, 495 (1968).

[24] S. J. Watzman, R. A. Duine, Y. Tserkovnyak, S. R. Boona, H. Jin, A. Prakash, Y. Zheng, and J. P. Heremans, Phys. Rev. B **94**, 144407 (2016).

[25] M. A. W. Schoen, J. Lucassen, H. T. Nembach, T. J. Silva, B. Koopmans, C. H. Back, and J. M. Shaw, Phys. Rev. B **95**, 134410 (2017).

[26] M. A. W. Schoen, J. Lucassen, H. T. Nembach, B. Koopmans, T. J. Silva, C. H. Back, and J. M. Shaw, Phys. Rev. B **95**, 134411 (2017).

[27] See Supplemental Material at http://link.aps.org/supplemental/10.1103/PhysRevB.98.020406 for more details on theory and experiment, which includes Refs. [36–70].

[28] P. Kim, L. Shi, A. Majumdar, and P. L. McEuen, Phys. Rev. Lett. **87**, 215502 (2001).

[29] B. Raquet, M. Viret, E. Sondergard, O. Cespedes, and R. Mamy, Phys. Rev. B **66**, 024433 (2002).

[30] M. V. Kamalakar, A. K. Raychaudhuri, X. Wei, J. Teng, and P. D. Prewett, Appl. Phys. Lett. **95**, 013112 (2009).

[31] R. P. Huebener, Phys. Rev. **171**, 634 (1968).

[32] In the fcc structure and for intermediate Co concentration the Fermi level is situated more closely above the step, while $\sigma(E)$ increases more strongly, when compared to the bcc structure. At elevated T the step contributes to $\mathcal{S}(T)$, resulting in an opposite curvature.

[33] D. T. Edmonds and R. G. Petersen, Phys. Rev. Lett. **2**, 499 (1959).

[34] T. M. Tritt, *Thermal Conductivity: Theory, Properties, and Applications* (Kluwer, New York, 2004).

[35] M. J. Laubitz and T. Matsumura, Can. J. Phys. **51**, 1247 (1973).

[36] International Centre of Diffraction Data, Powder Diffraction File 2, 48-1816 (http://www.icdd.com/); I. Baker, Thayer School of Engineering, Dartmouth College, 1997.

[37] International Centre of Diffraction Data, Powder Diffraction File 2, 15-0806 (http://www.icdd.com/); Natl. Bur. Stand. (U.S.) Monogr. **25**, 4, 10 (1966).

[38] P. P. Freitas and L. Berger, Phys. Rev. B **37**, 6079 (1988).

[39] M. Rubinstein, F. J. Rachford, W. W. Fuller, and G. A. Prinz, Phys. Rev. B **37**, 8689 (1988).

[40] J. W. C. De Vries, Thin Solid Films **167**, 25 (1988).

[41] N. W. Ashcroft and N. D. Mermin, *Solid State Physics* (Saunders College, New York, 1976).

[42] C. Ahn, K.-H. Shin, R. Loloee, J. Bass, and W. P. Pratt, Jr., J. Appl. Phys. **108**, 023908 (2010).

[43] H. Ebert, D. Ködderitzsch, and J. Minár, Rep. Prog. Phys. **74**, 096501 (2011).

[44] H. Ebert, J. Braun, D. Ködderitzsch, and S. Mankovsky, Phys. Rev. B **93**, 075145 (2016).

[45] H. Ebert *et al.*, The Munich SPR-KKR package, version 7.7, http://olymp.cup.uni-muenchen.de/ak/ebert/sprkkr (2017).

[46] P. Soven, Phys. Rev. **156**, 809 (1967).

[47] B. Velický, Phys. Rev. **184**, 614 (1969).

[48] B. Predel, *Phase Equilibria, Crystallographic and Thermodynamic Data of Binary Alloys: Ca-Cd-Co-Zr*, edited by O. Madelung, Landolt-Börnstein, New Series, Group IV Physical Chemistry, Vol. 5c (Springer, Berlin, 1993), Chap. Co-Fe (Cobalt-Iron), pp. 1–13.

[49] That is, not for the whole range between the pure metals as in Vegard's law.

[50] S. H. Vosko, L. Wilk, and M. Nusair, Can. J. Phys. **58**, 1200 (1980).

[51] O. K. Andersen, Phys. Rev. B **12**, 3060 (1975).

[52] R. Kubo, J. Phys. Soc. Jpn. **12**, 570 (1957).

[53] D. A. Greenwood, Proc. Phys. Soc. **71**, 585 (1958).

[54] L. Smrčka and P. Středa, J. Phys. C: Solid State Phys. **10**, 2153 (1977).

[55] W. H. Butler, Phys. Rev. B **31**, 3260 (1985).

[56] J. Banhart, R. Bernstein, J. Voitländer, and P. Weinberger, Solid State Commun. **77**, 107 (1991).

[57] J. Banhart, H. Ebert, P. Weinberger, and J. Voitländer, Phys. Rev. B **50**, 2104 (1994).

[58] S. Lowitzer, D. Ködderitzsch, and H. Ebert, Phys. Rev. B **82**, 140402(R) (2010).

[59] S. Lowitzer, M. Gradhand, D. Ködderitzsch, D. V. Fedorov, I. Mertig, and H. Ebert, Phys. Rev. Lett. **106**, 056601 (2011).

[60] A. Bastin, C. Lewiner, O. Betbeder-Matibet, and P. Nozieres, J. Phys. Chem. Solids **32**, 1811 (1971).

[61] A. Crépieux and P. Bruno, Phys. Rev. B **64**, 014416 (2001).

[62] D. Ködderitzsch, K. Chadova, and H. Ebert, Phys. Rev. B **92**, 184415 (2015).

[63] G. D. Mahan, *Many-Particle Physics*, 2nd ed. (Plenum, New York, 1993).

[64] M. Cutler and N. F. Mott, Phys. Rev. **181**, 1336 (1969).

[65] M. Jonson and G. D. Mahan, Phys. Rev. B **21**, 4223 (1980); **42**, 9350 (1990).

[66] S. Wimmer, D. Ködderitzsch, K. Chadova, and H. Ebert, Phys. Rev. B **88**, 201108(R) (2013).

[67] S. Wimmer, D. Ködderitzsch, and H. Ebert, Phys. Rev. B **89**, 161101(R) (2014).

[68] Y. Kakehashi and O. Hosohata, Phys. Rev. B **40**, 9080 (1989).

[69] W. H. Kleiner, Phys. Rev. **142**, 318 (1966).

[70] M. Seemann, D. Ködderitzsch, S. Wimmer, and H. Ebert, Phys. Rev. B **92**, 155138 (2015).